Electronic Supplementary Material (ESI) for Inorganic Chemistry Frontiers.

Supporting Information

Novel NiCoP nanoarray modified by NiFeCo layered double hydroxide quantum dots as highly-efficient bifunctional electrocatalysts in anion exchange membrane water electrolysis

Lina Li[a], Tao Yang[a,b*], Shuang Liu[a], Linlin Zhou[a], Kang Wang[a], Enhui Wang[a,b], Xiangtao Yu[a], Kuo-Chih Chou[a], Rui Guo[d], Zhen Ma[d], Xinmei Hou[a,b,c*]

[a]Institute for Carbon Neutrality, University of Science and Technology Beijing, Beijing 100083, China
[b]Institute of Steel Sustainable Technology, Liaoning Academy of Materials, Shenyang 110000, China
[c]Beijing Advanced Innovation Center for Materials Genome Engineering, University of Science and Technology Beijing, Beijing 100083, China
[d]Department of Cardiac Surgery, Peking University Third Hospital, Beijing, 100191, China.

Corresponding Author:
*Tao Yang, E-mail: yangtaoustb@ustb.edu.cn,
*Xinmei Hou, E-mail: houxinmeiustb@ustb.edu.cn
No. 30 Xueyuan Road, Haidian District, Beijing 100083 P. R. China.

1. Experimental section

1.1 Electrochemical measurements

1.2 The AEM water electrolysis test

1.3 DFT Calculations

2. Supplementary Figures

Fig. S1. AFM spectrum and image of LDHQDs.

Fig. S2. Top view of models (a) NiCoP, (b) NiFeCo-LDH, and (c) NiFeCo-LDH/NiCoP. Side view of models (d) NiCoP, (e) NiFeCo-LDH, and (f) NiFeCo-LDH/NiCoP.

Fig. S3. Cyclic voltammetry curves of (a) NiCoP NA. (b) LDHQDs, and (c) LDHQDs/NiCoP NA in 1 M KOH under different scan rates for HER (from 2mV/s to 10 mV/s).

Fig. S4. After HER stability test performance of LDHQDs/NiCoP NA (a) XPS full spectrum and XPS spectrum of (b) Ni 2p, (c) Co 2p, (d) Fe 2p, (e) P 2p and (f) O 1s.

Fig. S5. Cyclic voltammetry curves of (a) NiCoP NA. (b) LDHQDs, (c) LDHQDs/NiCoP NA in 1 M KOH under different scan rates for OER (from 2mV/s to 10 mV/s).

Fig. S6. After OER stability test performance of LDHQDs/NiCoP NA (a) XPS full spectrum and XPS spectrum of (b) Ni 2p, (c) Co 2p, (d) Fe 2p, (e) P 2p and (f) O 1s.

Fig. S7. The overall water splitting LSV plots of LDHQDs/NiCoP NA before and after stability test.

Fig. S8. (a) SEM image and (b) XRD pattern of LDH-QDs/NiCoP NA after 50 h durability test.

Fig. S9. The SEM images of LDHQDs/NiCoP NA after AEM electrolyzer stability test

(a) cathode and (b) anode test.

Fig. S10. The XRD pattern of LDHQDs/NiCoP NA after AEM electrolyzer stability test (a) cathode and (b) anode test.

3. Supplementary tables

Table S1. Comparison of other multifunctional electrocatalysts in 1 M KOH for HER.

Table S2. The parameters utilized in the mass activity calculation of NiCoP NA, LDHQDs and LDHQDs/NiCoP NA in HER

Table S3. Comparison of other multifunctional electrocatalysts in 1 M KOH for OER.

Table S4. The parameters utilized in the mass activity calculation of NiCoP NA, LDHQDs and LDHQDs/NiCoP NA in OER

Table S5. Comparison of other multifunctional electrocatalysts in 1 M KOH for overall water splitting.

Table S6. Comparison of LDHQDs/NiCoP AEM electrolyzer performance with previously reported AEM electrolyzer in 1 M KOH

1. Experimental section

1.1 Electrochemical measurements

The electrocatalytic properties were evaluated using a standard three-electrode system on a CHI 760E workstation. The working electrode area was 1×1 cm^2, with a graphite rod serving as the counter electrode and a Hg/HgO electrode as the reference electrode. Prior to testing, the working electrodes were electrochemically activated 50 times at a current density of 50 mA/cm^2 using cyclic voltammetry (CV). Linear sweep voltammetry (LSV) curves were obtained at a sweep rate of 5 mV/s and corrected with 90% internal resistance (*IR*) compensation. All measured potentials were converted to potentials against a reversible hydrogen electrode (RHE) using the Nernst equation ($E_{RHE} = E_{Hg/HgO} + 0.059pH + 0.098$ V). Electrochemical impedance spectroscopy (EIS) was performed at a frequency range of 10^6 to 10^{-2} Hz and at 1.6 V vs. RHE. The Tafel slope was calculated by fitting the linear portion of the Tafel graph to the Tafel equation ($\eta = a + b \log(j)$)[1]. To determine the electrochemical active surface area (ECSA), the double-layer capacitance (C_{dl}) was measured using cyclic voltammetry (CV) at different scan rates ranging from 2 to 10 mV/s. C_{dl} was determined byplotting the current difference ($\Delta j/2$) against the sweep rate (mV/s). The mass activity was determined by normalizing the current density to the mass of the electrocatalyst. Catalyst loads of NiCoP NA, LDHQDs and LDHQDs/NiCoP NA were uniformly recorded on the NFs. Geometric dimension of NiCoP NA, LDHQDs and LDHQDs/NiCoP NA were 1*1 cm^2. Catalyst loads of NiCoP NA, LDHQDs and LDHQDs/NiCoP NA were 1.7 mg, 1.5 mg, 1.4 mg

1.2 The AEM water electrolysis test

The AEM system consists of the gas diffusion electrodes, PTFE gaskets and AEM, FAA-3-PK-130. Both anodic and cathodic electrodes were fabricated by the gas diffusion electrode method. To assemble the AEM system, FAA-3-PK-130 was first soaked in a 1 M KOH solution for 24 hours to exchange Cl^- ions with OH^- ions. Electrically insulating gaskets were used to prevent any leakage of liquid or gas. The cell assembly was tightened using a torque of approximately 4 Nm. A 1 M KOH solution was then circulated through the anodic side of the system via a peristaltic pump. Polarization curves were recorded by varying the voltage from 1.0 V to 2.5 V at water temperatures ranging from 30 ºC to 80 ºC under ambient pressure. Additionally, a stability test was conducted by maintaining a constant cell voltage of 2 V at 80 ºC.

1.3 DFT Calculations

DFT calculations were carried out using the generalized gradient approximation (GGA) within the Vienna Ab Initio Simulation Package (VASP). The PBE functional [2,3] was employed to describe the exchange-correlation functional. The plane-wave basis cutoff energy was set to 460 eV, and the convergence threshold was set to 0.02 eV $Å^{-1}$ in force and 10^{-6} eV in energy. For the structure optimization and electronic properties of NiFeCo-LDH/NiCoP, a 3×3×1 K-mesh in the Brillouin zone was utilized. To prevent vertical interactions between adjacent slabs, a vacuum layer of 25 Å was included.

Utilizing DFT calculations, the molecular-level interaction between NiFeCo-LDH and NiCoP was investigated. To ensure model stability and primary cell size, on the (001) surface of NiCoP, a NiOOH sample doped with a ratio of Ni:Co:Fe = 1:1:1 was

fabricated. The total charge density of NiFeCo-LDH/NiCoP is subtracted from the charge density of NiFeCo-LDH and NiCoP to obtain the charge density difference distribution between the two phases. DFT calculations were performed to evaluate their surface energetics, with electron gain represented by yellow regions and electron loss indicated by blue regions.

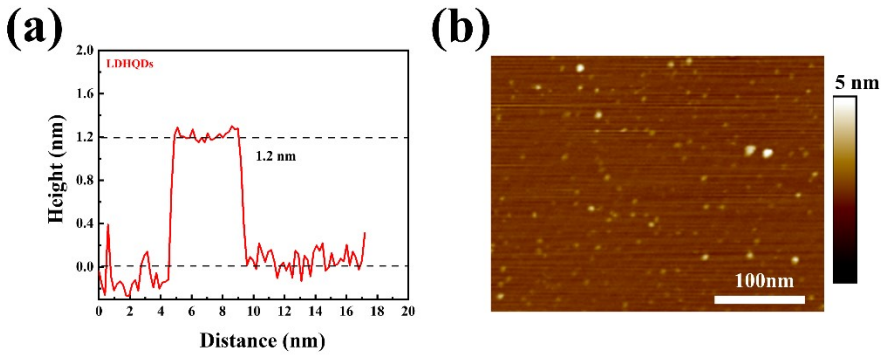

Fig. S1. AFM spectrum and image of LDHQDs.

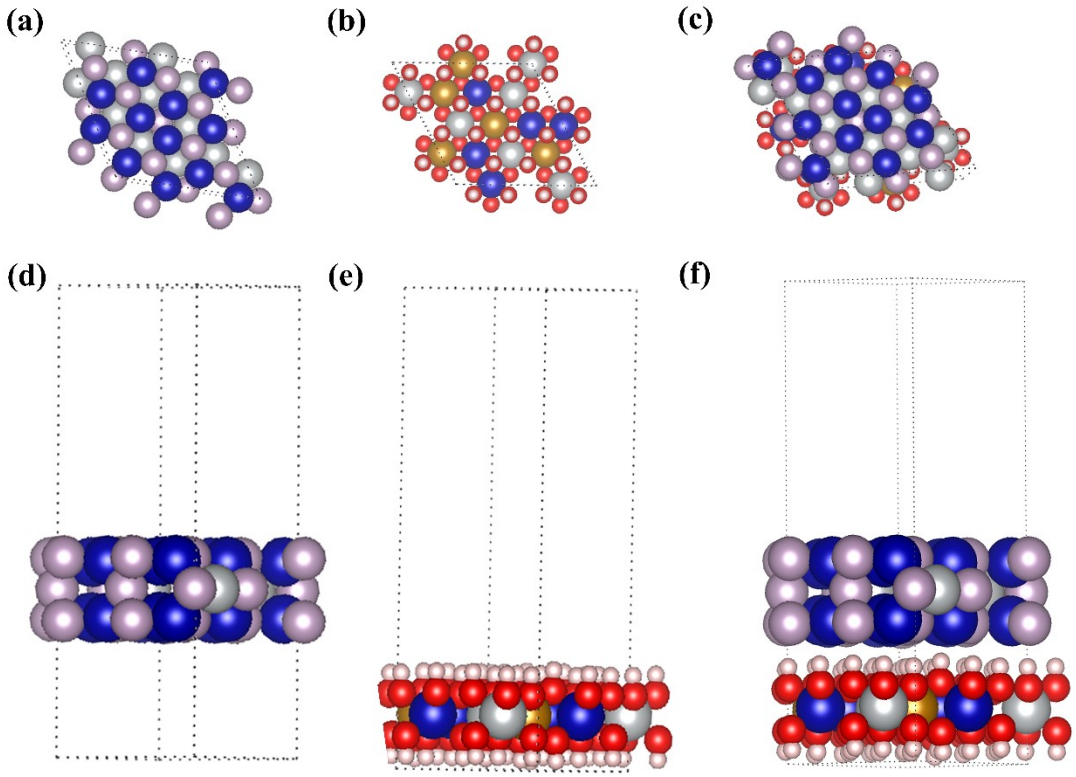

Fig. S2. Top view of models (a) NiCoP, (b) NiFeCo-LDH, and (c) NiFeCo-LDH/NiCoP. Side view of models (d) NiCoP, (e) NiFeCo-LDH, and (f) NiFeCo-LDH/NiCoP.

Table S1. Comparison of other multifunctional electrocatalysts in 1 M KOH for HER.

Materials	Overpotential (η_{10}, mV)	Overpotential (η_{1000}, mV)	Ref.
CoMo-LDH	115	-	[4]
CNT@NiCo/CP*	82	-	[5]
NiAl-LDH	90	-	[6]
Co_9S_8@NiFe-LDH HAs/NF**	145	-	[7]
$NiCo_{(nf)}$-P***	87	317	[8]
Mo-NiS@NiFe LDH/NF	107	-	[9]
CeO_2-NiCoP	84	242	[10]
$NiFeCoS_x$@$FeNi_3$	88	-	[11]
$Ni_{0.8}Fe_{0.2}$-AHNA****	21	207	[12]
LDHQDs/NiCoP NA	75	263	This Work

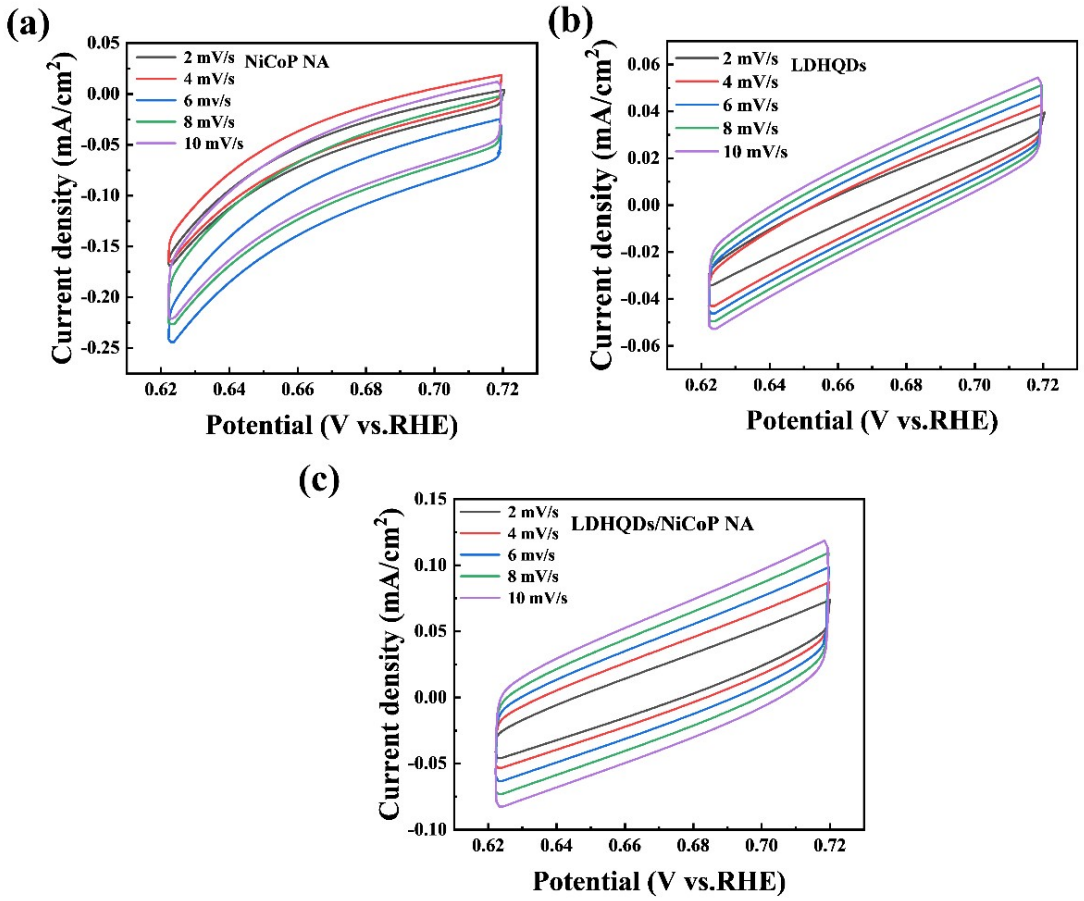

Fig. S3. Cyclic voltammetry curves of (a) NiCoP NA. (b) LDHQDs, and (c) LDHQDs/NiCoP NA in 1 M KOH under different scan rates for HER (from 2mV/s to 10 mV/s).

Table S2. The parameters utilized in the mass activity calculation of NiCoP NA, LDHQDs and LDHQDs/NiCoP NA in HER

	Overpotential (mV)	Current density (mA/cm^2)	Catalyst loads (mg)	Mass activity (A/g)
NiCoP NA	250	400	1.7	235.3
LDHQDs	250	111	1.5	74.0
LDHQDs/ NiCoP NA	250	860	1.4	616.3

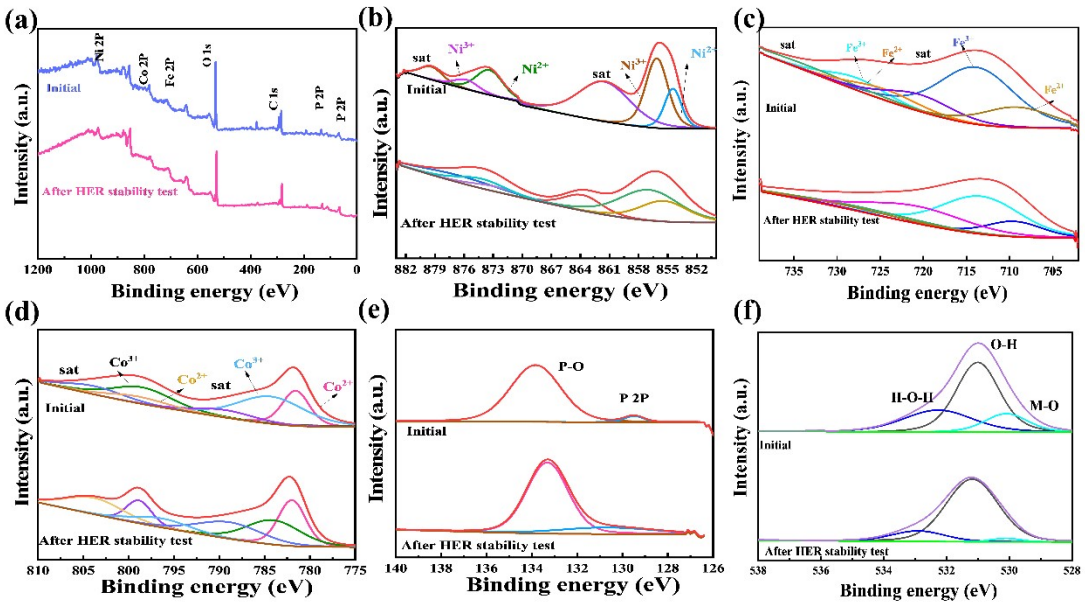

Fig. S4. After HER stability test performance of LDHQDs/NiCoP NA (a) XPS full spectrum and XPS spectrum of (b) Ni 2p, (c) Co 2p, (d) Fe 2p, (e) P 2p and (f) O 1s.

Table S3. Comparison of other multifunctional electrocatalysts in 1 M KOH for OER.

Materials	Overpotential (η_{10}, mV)	Overpotential (η_{1000}, mV)	Ref.
CoMo-LDH	290	-	[4]
CNT@NiCo/CP*	230	-	[5]
NiAl-LDH	180	-	[6]
Co_9S_8@NiFe-LDH HAs/NF**	190	-	[7]
$NiCo_{(nf)}$-P***	205	416	[8]
Mo-NiS@NiFe LDH/NF	184	-	[9]
$NiFeCoS_x$@$FeNi_3$	210	-	[11]
$Ni_{0.8}Fe_{0.2}$–AHNA****	190	258	[12]
LDHQDs/NiCoP NA	203	330	This Work

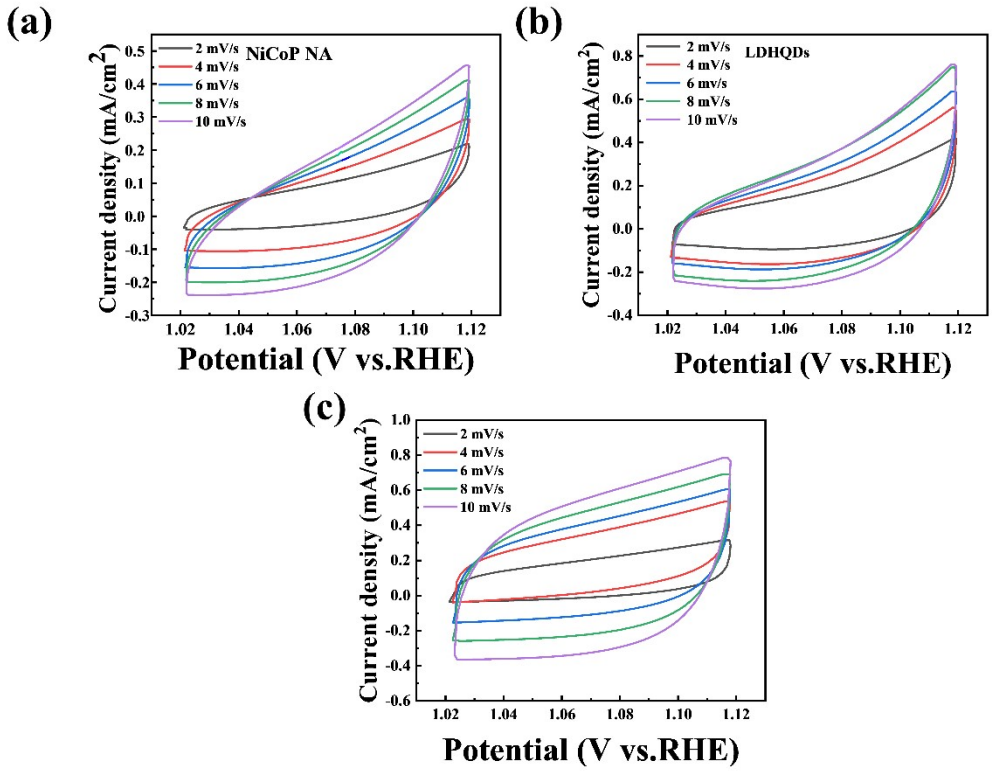

Fig. S5. Cyclic voltammetry curves of (a) NiCoP NA. (b) LDHQDs, (c) LDHQDs/NiCoP NA in 1 M KOH under different scan rates for OER (from 2mV/s to 10 mV/s).

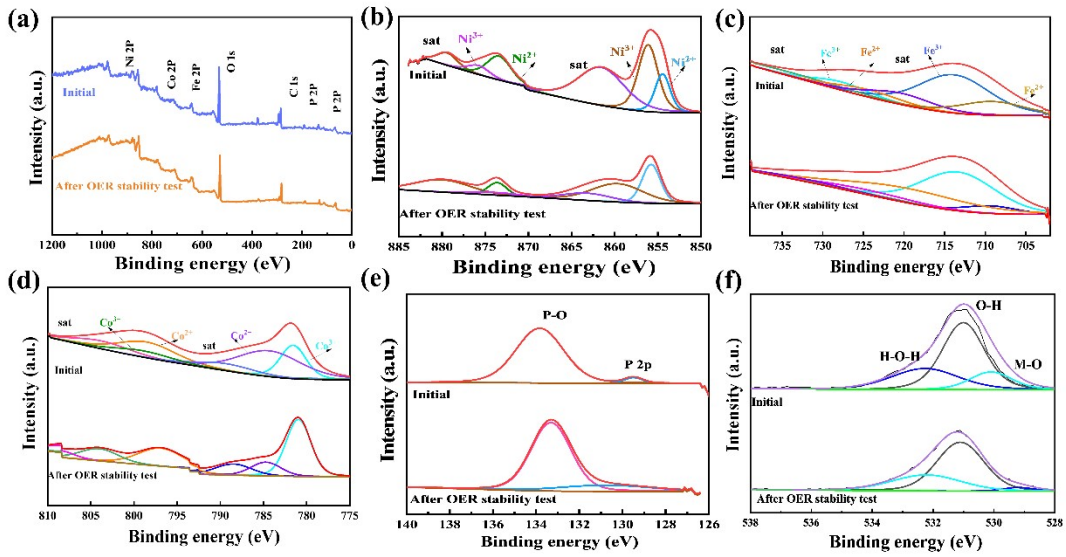

Fig. S6. After OER stability test performance of LDHQDs/NiCoP NA (a) XPS full spectrum and XPS spectrum of (b) Ni 2p, (c) Co 2p, (d) Fe 2p, (e) P 2p and (f) O 1s.

Table S4. The parameters utilized in the mass activity calculation of NiCoP NA, LDHQDs and LDHQDs/NiCoP NA in OER

	Overpotential (mV)	Current density (mA/cm^2)	Catalyst loads (mg)	Mass activity (A/g)
NiCoP NA	350	275	1.7	161.7
LDHQDs	350	247	1.5	164.7
LDHQDs/ NiCoP NA	350	988	1.4	705.7

Table S5. Comparison of other multifunctional electrocatalysts in 1 M KOH for overall water splitting.

Materials	Potential (η_{10}, V)	Potential (η_{1000}, V)	Ref.
CoMo-LDH	1.63	-	4
CNT@NiCo/CP*	1.58	-	5
NiAl-LDH	1.5	-	6
Co_9S_8@NiFe-LDH HAs/NF**	1.585	-	7
$NiCo_{(nf)}$-P***	-	1.94	8
Mo-NiS@NiFe LDH/NF	1.54	-	9
CeO_2-NiCoP	-	1.8	10
$Ni_{0.8}Fe_{0.2}$–AHNA****	1.41	1.76	12
LDHQDs/NiCoP NA	1.47	1.69	This Work

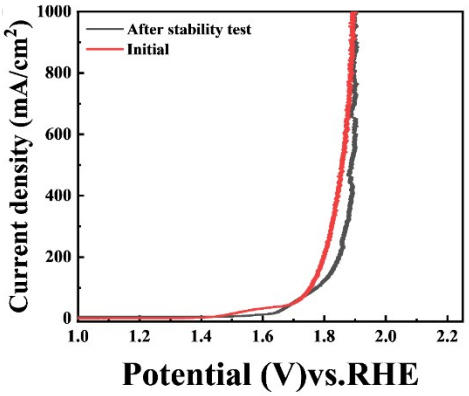

Fig. S7. The overall water splitting LSV plots of LDHQDs/NiCoP NA before and after stability test.

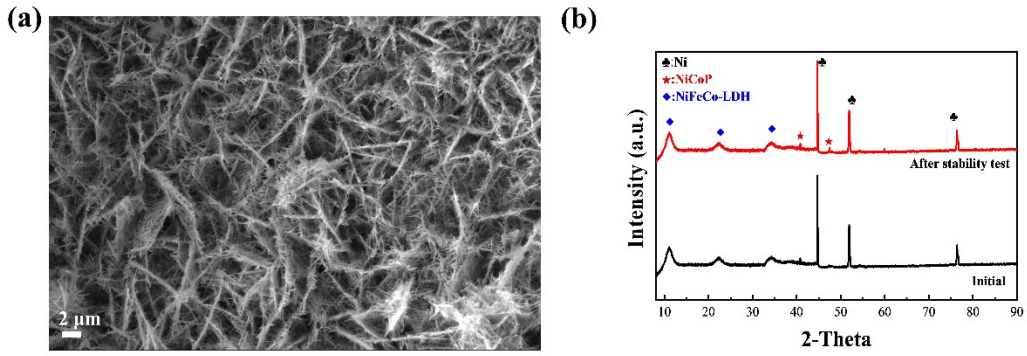

Fig. S8. (a) SEM image and (b) XRD pattern of LDH-QDs/NiCoP NA after 50 h durability test.

Table S6. Comparison of LDHQDs/NiCoP AEM electrolyzer performance with previously reported AEM electrolyzer in 1 M KOH.

OER	HER	Temperature (ºC)	Cell voltage (V)	Current density (A/cm^2)	Ref.
Ni/CP	Ni/CP	-	1.9	0.15	[13]
Co_2Fe	Pt/C	-	1.9	0.13	[14]
$Ni_{12}P_5/Ni_3(PO_4)_2$ -HS*****	$Ni_{12}P_5/Ni_3(PO_4)_2$ -HS	50	1.8	0.357	[15]
NiFe-LDH	NiFe-LDH	50	2	0.5	[16]
NiFe LDH-PMo	Ni@NiFe LDH	60	1.7	0.2	[17]
NiFe LDH-PMo	Ni@NiFe LDH	25	1.89	0.2	[17]
LDHQDs /NiCoP	LDHQDs /NiCoP	80	2	0.57	This Work
LDHQDs /NiCoP NA	LDHQDs /NiCoP NA	80	2.28	1	This Work
LDHQDs /NiCoP NA	LDHQDs /NiCoP NA	60	2.5	1	This Work

*: carbon nanotube (CNT) load NiCoP on carbon paper

**: Co_9S_8@NiFe-LDH core-branch hierarchical architectures supported on nickel foam

***: metal–organic framework derived NiCoP nanoflakes

****: NiFe oxy-hdroxide@NiFe alloy nanowire array

*****: $Ni_{12}P_5/Ni_3(PO_4)_2$ hollow spheres

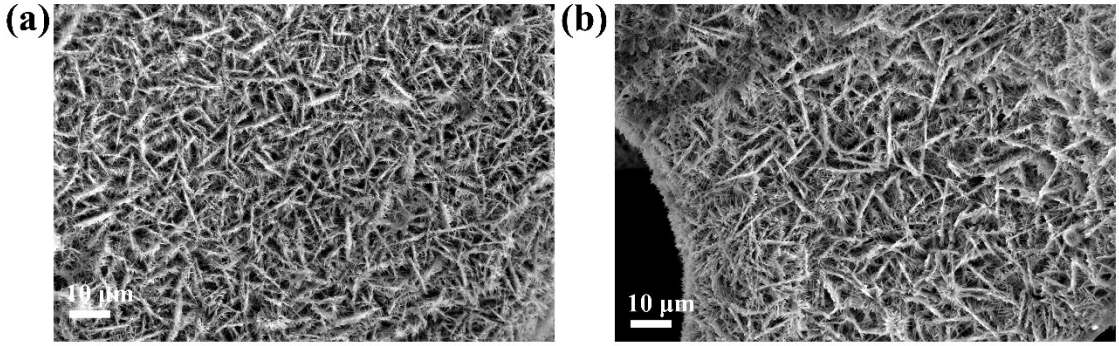

Fig. S9. The SEM images of LDHQDs/NiCoP NA after AEM electrolyzer stability test (a) cathode and (b) anode test.

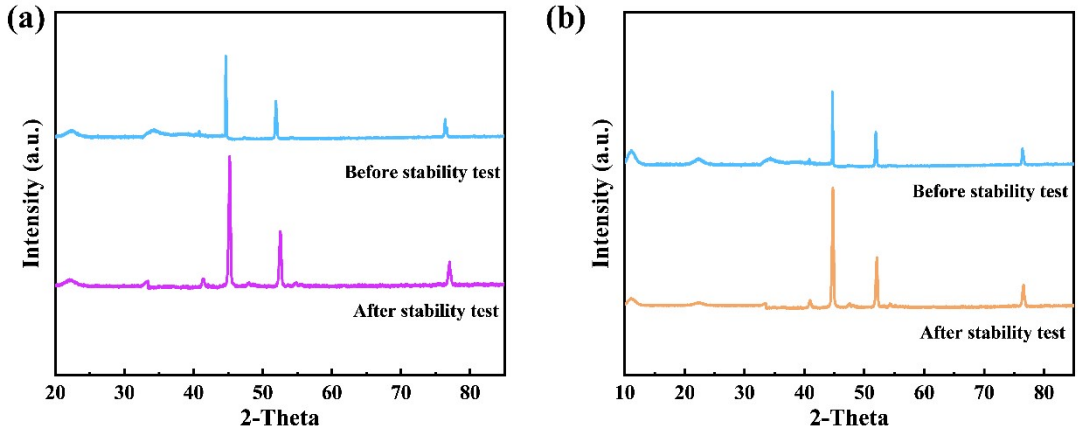

Fig. S10. The XRD pattern of LDHQDs/NiCoP NA after AEM electrolyzer stability test (a) cathode and (b) anode test.

References

1. J. Tafel, Über die Polarisation bei kathodischer Wasserstoffentwicklung, *Zeitschrift für Physikalische Chemie*, 1905, **50U**, 641-712.

2. G. Kresse and J. Furthmuller, Efficient iterative schemes for ab initio total-energy calculations using a plane-wave basis set, *Phys Rev B Condens Matter*, 1996, **54**, 11169-11186.

3. J. P. Perdew, K. Burke and M. Ernzerhof, Generalized Gradient Approximation Made Simple, *Physical Review Letters*, 1996, **77**, 3865-3868.

4. J. Bao, Z. Wang, J. Xie, L. Xu, F. Lei, M. Guan, Y. Huang, Y. Zhao, J. Xia and H. Li, The CoMo-LDH ultrathin nanosheet as a highly active and bifunctional electrocatalyst for overall water splitting, *Inorganic Chemistry Frontiers*, 2018, **5**, 2964-2970.

5. Z. Wang, C. Wei, X. Zhu, X. Wang, J. He and Y. Zhao, A hierarchical carbon nanotube forest supported metal phosphide electrode for efficient overall water splitting, *Journal of Materials Chemistry A*, 2021, **9**, 1150-1158.

6. L. Feng, Y. Du, J. Huang, L. Cao, L. Feng, Y. Feng, Q. Liu, D. Yang and K. Kajiyoshi, Nanoporous NiAl-LDH nanosheet arrays with optimized Ni active sites for efficient electrocatalytic alkaline water splitting, *Sustainable Energy & Fuels*, 2020, **4**, 2850-2858.

7. Y. Lu, C. Liu, Y. Xing, Q. Xu, A. M. S. Hossain, D. Jiang, D. Li and J. Zhu, Synergistically integrated Co9S8@NiFe-layered double hydroxide core-branch hierarchical architectures as efficient bifunctional electrocatalyst for water splitting, *Journal of Colloid and Interface Science*, 2021, **604**, 680-690.

8. Z. Xu, C.-L. Yeh, J.-L. Chen, J. T. Lin, K.-C. Ho and R. Y.-Y. Lin, Metal–Organic Framework-Derived 2D NiCoP Nanoflakes from Layered Double Hydroxide Nanosheets for Efficient Electrocatalytic Water Splitting at High Current Densities, *ACS Sustainable Chemistry & Engineering*, 2022, **10**, 11577-11586.

9. S. Qiu, B. Zhang, X. Wang, J. Huang, G. Zhao, M. Ding and X. Xu, Interface strong-coupled 3D Mo-NiS@Ni-Fe LDH flower-cluster as exceptionally efficient electrocatalyst for water splitting in wide pH range, *Journal of Colloid and Interface Science*, 2023, **641**, 277-288.

10. X. Guo, M. Li, L. Qiu, F. Tian, L. He, S. Geng, Y. Liu, Y. Song, W. Yang and Y. Yu, Engineering electron redistribution of bimetallic phosphates with CeO2 enables high-performance overall water splitting, *Chem. Eng. J. (Lausanne)*, 2023, **453**, 139796.

11. J. Shen, Q. Li, W. Zhang, Z. Cai, L. Cui, X. Liu and J. Liu, Spherical Co3S4 grown directly on Ni–Fe sulfides as a porous nanoplate array on FeNi3 foam: a highly efficient and durable bifunctional catalyst for overall water splitting, *Journal of Materials Chemistry A*, 2022, **10**, 5442-5451.

12. C. Liang, P. Zou, A. Nairan, Y. Zhang, J. Liu, K. Liu, S. Hu, F. Kang, H. J. Fan and C. Yang, Exceptional performance of hierarchical Ni–Fe oxyhydroxide@NiFe alloy nanowire array electrocatalysts for large current density water splitting, *Energy & Environmental Science*, 2020, **13**, 86-95.

13. S. H. Ahn, B.-S. Lee, I. Choi, S. J. Yoo, H.-J. Kim, E. Cho, D. Henkensmeier, S. W. Nam, S.-K. Kim and J. H. Jang, Development of a membrane electrode assembly

for alkaline water electrolysis by direct electrodeposition of nickel on carbon papers, *Applied Catalysis B: Environmental*, 2014, **154-155**, 197-205.

14. G.-C. Chen, T. H. Wondimu, H.-C. Huang, K.-C. Wang and C.-H. Wang, Microwave-assisted facile synthesis of cobaltiron oxide nanocomposites for oxygen production using alkaline anion exchange membrane water electrolysis, *International Journal of Hydrogen Energy*, 2019, **44**, 10174-10181.

15. J. Chang, Q. Lv, G. Li, J. Ge, C. Liu and W. Xing, Core-shell structured Ni12P5/Ni3(PO4)2 hollow spheres as difunctional and efficient electrocatalysts for overall water electrolysis, *Applied Catalysis B: Environmental*, 2017, **204**, 486-496.

16. H. Li, M. R. Kraglund, A. K. Reumert, X. Ren, D. Aili and J. Yang, Poly(vinyl benzyl methylpyrrolidinium) hydroxide derived anion exchange membranes for water electrolysis, *Journal of Materials Chemistry A*, 2019, **7**, 17914-17922.

17. Z. Cai, P. Wang, J. Zhang, A. Chen, J. Zhang, Y. Yan and X. Wang, Reinforced Layered Double Hydroxide Oxygen-Evolution Electrocatalysts: A Polyoxometallic Acid Wet-Etching Approach and Synergistic Mechanism, *Adv. Mater. (Weinheim, Ger.)*, 2022, **34**, 2110696.